Atmos. Chem. Phys., 26, 3637–3652, 2026
https://doi.org/10.5194/acp-26-3637-2026

Atmospheric Chemistry and Physics
Open Access
EGU

Parametrizing the mixing by clear air turbulence in the chemistry climate model EMAC and its respective radiative impact

Chun Hang Chau[1], **Peter Hoor**[1], **Katharina Kaiser**[2], **and Holger Tost**[1]

[1]Institute for Atmospheric Physics, Johannes Gutenberg University Mainz, Mainz, Germany
[2]Aerosol Chemistry Department, Max Planck Institute for Chemistry, Mainz, Germany

Correspondence: Chun Hang Chau (cchau@uni-mainz.de)

Received: 30 October 2025 – Discussion started: 12 November 2025
Revised: 28 February 2026 – Accepted: 4 March 2026 – Published: 11 March 2026

Abstract. The Earth's radiation budget is found to be sensitive to changes in the upper troposphere and lower stratosphere (UTLS) chemical composition. Stratosphere-troposphere exchange is the major process that influences the UTLS chemical composition with remaining uncertainties in current climate-chemistry models. This exchange could be e.g., facilitated by clear air turbulence (CAT), as it leads to diabatic mixing of chemical tracers between stratosphere and troposphere. In this work, we examine the potential impact of vertical mixing by CAT on the UTLS chemical composition and its corresponding radiative impact by implementing a newly developed submodel parametrizing turbulent mixing in the free troposphere and stratosphere within the chemistry climate model EMAC. This submodel parametrizes the vertical mixing by CAT based on a newly introduced turbulence diagnostic Modified CAT Index (MoCATI). MoCATI shows a comparable performance with the well-established Ellrod-Knox index. Simulations are conducted with EMAC under the Quasi Chemistry transport Model (QCTM) mode to examine the sole impact of mixing, without taking the potential feedback into account. Results show that the radiatively active ozone in the UTLS is most sensitive to the vertical mixing of CAT and is significantly reduced by 10 % to 20 % by the CAT submodel. This modification is not a pure result of the physical mixing but also the chemical feedback of other tracer distributions modified by CAT. The tracer mixing through CAT also changes the atmospheric chemistry by shortening the CH_4 lifetime and changing the O_3 becoming more sensitive to NO_x. It also leads to potential surface radiative heating and radiative cooling at the top of the atmosphere. The global average radiative effect is about $-0.2\,W\,m^{-2}$ without considering water vapour.

1 Introduction

The upper troposphere and lower stratosphere (UTLS) plays a crucial role on the Earth's radiation budget (Forster et al., 2021). Changes in the chemical composition in the UTLS could lead to changes via the radiation locally as well as at the surface. Ozone and water vapour near the tropopause are found to have more radiative influence on the surface compared to other well-mixed greenhouse gases (Riese et al., 2012; Lacis et al., 1990). Removal of ozone above the tropopause could lead to local cooling (Randel et al., 2007). The surface temperature is also highly sensitive to changing ozone concentration in the UTLS, increasing ozone in this region could increase the surface temperature (Forster and Shine, 1997; Lacis et al., 1990). Water vapour also has complex impacts on the Earth's radiation. Increasing stratospheric water vapour could lead to local cooling (Forster and Shine, 1999; Randel et al., 2007) and surface warming (Solomon et al., 2010).

Since stratosphere-troposphere exchange (STE) is one of the major processes that influence the UTLS chemical composition (Holton et al., 1995; Stohl et al., 2003), it is crucial to improve the representation of STE in the model. Previous studies show that the simulated upper tropospheric ozone budget depends on the model representation of STE (Stevenson et al., 2006). A key feature for STE is the oc-

currence of vertical shear, which has recently been shown to form a layer with high probability of shear occurrence near the local tropopause (Kaluza et al., 2021). Vertical shear is a key mechanism to initiate turbulence and thus mixing. Turbulent mixing in the UTLS is one of the pathways of the STE (Holton et al., 1995) and it is not represented in several state-of-the-art chemistry climate models, such as EMAC (Jöckel et al., 2016). In ECHAM5, the base model of EMAC, the turbulence scheme was designed for the surface boundary layer only; it sets a constant asymptotic mixing length in the boundary layer and simply assumes it decreases exponentially with height, approaching 1 m in the lower stratosphere (Roeckner et al., 2003), resulting in a dampening effect on the turbulence in the UTLS, which normally does not mix tracers significantly. Therefore, this study presents a parametrization of tracer mixing by clear air turbulence (CAT), which is commonly found in the UTLS and could lead to rapid mixing of the chemical composition between the troposphere and stratosphere (Dutton and Panofsky, 1970; Esler and Polvani, 2004; Traub and Lelieveld, 2003).

CAT represents the turbulence in the free atmosphere that occurs in a cloud-free region (Ellrod et al., 2003). Kelvin-Helmholtz instability, which is a result of vertical wind shear (Kunkel et al., 2019; Dutton and Panofsky, 1970; Richardson, 1920), is the major mechanism that leads to CAT formation (Watkins and Browning, 1973; Ellrod and Knapp, 1992; Dutton and Panofsky, 1970). Considering turbulence is not explicitly represented by global scale numerical models, CAT is usually forecast using diagnostics that are based on related larger-scale mechanisms. A previous study has shown that turbulence diagnostics are reliable for forecasting CAT operationally in NWP models (Sharman et al., 2006). However, each of the turbulence diagnostics has its own advantages and disadvantages. Ellrod index (TI) is one of the most commonly used CAT diagnostics in the aviation sector. It is based on the meso-scale condition that leads to CAT including vertical wind shear and deformation of the horizontal wind (Ellrod and Knapp, 1992). The Ellrod-Knox index is the improved version of the TI by introducing an additional divergence trend term (Ellrod and Knox, 2010). (Williams and Storer, 2022) confirmed that turbulence diagnostics are capable of diagnosing CAT and its response to climate change in climate models with coarser resolution. Another recent study from (Chau et al., 2025) shows that the turbulence diagnostic calculated from the grid scale wind field matches well with a detailed sub-grid scale turbulence scheme in the UTLS for a regional forecast model.

CAT is expected to become more frequent and intense under climate change because of the more sheared atmosphere (Williams, 2017). The vertical wind shear at 250 hPa in the North Atlantic region has increased by 15 % between 1979 and 2017 (Lee et al., 2019). Several studies show that the strength of CAT will be stronger in the North Atlantic and East Asia under different climate change scenarios (Williams and Joshi, 2013; Smith et al., 2023; Hu et al., 2021). Therefore, there is a necessity to study how CAT could potentially change the atmosphere. Previous studies have examined the sensitivity of the vertical mixing in a Lagrangian approach, concluding that water vapour and ozone are most sensitive to vertical mixing and lead to a significant impact on the radiation budget (Riese et al., 2012). The main objective of this study is to examine the potential impact of vertical turbulent mixing by CAT on the UTLS chemistry and radiation in an Eulerian approach. For this purpose, we introduce a new EMAC submodel to parametrize the CAT-induced vertical mixing of tracers in the UTLS. In order to examine the sole impact of CAT but not its feedback, the simulations are conducted in a Quasi Chemistry transport Model (QCTM) mode (Deckert et al., 2011) to ensure identical model dynamics independent of the chemical composition.

This paper consists of three further sections after the introduction: Sect. 2 introduces the EMAC model configuration and the newly developed CAT submodel. Section 3 presents the results and discusses the CAT submodel in terms of redistributing chemical composition and radiative impact. Section 4 summarises the findings and draws conclusions with a future outlook.

2 Method

2.1 EMAC Model Description

EMAC (ECHAM/MESSy Atmospheric Chemistry; Jöckel et al., 2006; Jöckel et al., 2010) is a state-of-the-art chemistry climate model that allows flexible model configuration via different submodels. It combines the general circulation model ECHAM5 (Roeckner et al., 2003) with the Modular Earth Submodel System (MESSy; Jöckel et al., 2005) which allows users to include different physical and chemical processes via a namelist interface. EMAC is also able to operate in quasi chemistry-transport model mode (QCTM; Deckert et al., 2011), which allows decoupling between chemistry and dynamics in the model, suppressing the feedback between chemistry and dynamics to better quantify the signal from a particular process. For our study, EMAC is operated in T42L90MA resolution (Giorgetta et al., 2006). It is a configuration designed for the middle atmosphere with a horizontal resolution of T42 (approximately $2.8° \times 2.8°$) and 90 vertical hybrid pressure levels up to 0.01 hPa. The vertical resolution in the UTLS is approximately 400 to 500 m.

2.2 Experimental setup

Two simulations: QCTM-MIX and QCTM-NOMIX are performed in this work. Two decadal simulations with gas-phase chemistry are performed using the EMAC-QCTM to examine the long-term impact of the CAT submodel without the dynamical feedback from chemistry. Both simulations are performed with the perpetual year of 2014 for 10 years, pre-

scribing the emission, sea surface temperature and sea ice concentration of 2014 repetitively. The chemistry setup is adapted from the RC1-base-07 of Jöckel et al. (2016), which is the Ref-C1 of the CCMI (Eyring et al., 2013), a free-running historical hindcast. The emissions are prescribed by the CCMI-2022 Ref-D1 (Plummer et al., 2021), which is a historical hindcast. The sea surface temperature and sea ice concentration are prescribed by the AMIP-II data set (Taylor et al., 2000), the monthly means computed from model output, which agree with the observations. Both simulations are initialized with the ERA-Interim reanalysis data (Dee et al., 2011).

QCTM-NOMIX with the CAT submodel disabled is used as a reference simulation, while the QCTM-MIX enables the CAT submodel to examine the impact of the CAT tracer mixing. The details for the CAT submodel are discussed in Sect. 2.3.

2.2.1 Radiation (RAD) submodel of EMAC

In EMAC, the radiation scheme (RAD) is a re-implementation of the ECHAM5/ECHAM6 radiation codes with more flexibility (Dietmüller et al., 2016). It calculates the radiation depending on radiatively active tracers, including CO_2, CH_4, O_3, N_2O, CFC-11 and CFC-12. It also requires input parameters like water vapour, cloud cover, clear-sky index, cloud optical properties, aerosol optical properties, and orbital parameters provided by the model. RAD allows for both online and offline radiation calculations, i.e., using either prognostic variables (tracers) or external data sources for the radiatively active species. To run EMAC in the QCTM mode, climatological values or distributions of the radiatively active gases are utilised for the radiation calculation to decouple the feedback between the gases and the radiation scheme. Water vapour also needs to be decoupled from the chemistry to prevent inconsistency in model dynamics. Therefore, the mixing scheme of the new submodel CAT (Sect. 2.3) does not include water vapour at this stage. RAD also provides an option to calculate the radiative disturbances from different sets of radiatively active gases by calling the radiation routine multiple times within one model time step. The temperature feedback will be provided by the first call. This option provides an opportunity to examine the pure radiative impact of the CAT mixing without dynamical feedback within EMAC-QCTM. In both simulations, a total of six calls are set. For the first call, which provides the temperature feedback of the model, prescribed values for the radiatively active gases are used. For the second call, the radiation calculation uses all the online interactive chemistry output provided by EMAC. To isolate the individual contribution of each gas, four additional radiation calls are set. In each call, only the specified gas uses the online output from the model, the other gases remain unchanged using the prescribed values. Detailed information about the applied values and the dataset is given in Table 1. The prescribed values for CO_2, CH_4, N_2O, CFC-11 and CFC-12 are provided by the Global Monitoring Laboratory of NOAA. The prescribed O_3 is taken from the climatology of (Paul et al., 1998).

2.3 New MESSy submodel CAT for clear air turbulence mixing

This section introduces the newly developed submodel CAT of MESSy. The new CAT submodel is developed to parametrize the vertical mixing of tracers caused by clear air turbulence in the UTLS. It allows vertical mixing of tracers based on a 2-layer mixing algorithm between 500 to 70 hPa, considering that CAT occurs most frequently in the UTLS (Dutton and Panofsky, 1970). At pressure levels below 70 hPa, vertical tracer mixing by turbulence is strongly suppressed due to the strong static stability. At pressures higher than 500 hPa, deep tropopause fold intrusions might occur and lead to tracer mixing; however, such structures are usually not represented well in a typical EMAC setup with a coarse horizontal resolution (e.g. T42 and T63). Therefore, the CAT parametrization is switched off for pressure lower than 70 hPa and higher than 500 hPa, considering the limited computational resources and to avoid overlap with the boundary layer parametrization scheme. The mixing scheme of CAT follows a typical K-theory for turbulence fluxes and uses a turbulence diagnostic (CAT Index) to serve as a mixing coefficient and provides two options for now: the Ellrod-Knox index (Ellrod and Knox, 2010) and a newly introduced Modified CAT Index (MoCATI) specifically modified for tracer mixing. The Ellrod-Knox index is a widely tested and used turbulence diagnostic, which is based on the grid scale wind field data including deformation (DEF), vertical wind shear (VWS), and divergence trend (DVT):

$$\begin{aligned}\text{Ellrod-Knox index} = & \underbrace{\left[\left(\frac{\partial u}{\partial x}-\frac{\partial v}{\partial y}\right)^2+\left(\frac{\partial v}{\partial x}+\frac{\partial u}{\partial y}\right)^2\right]^{\frac{1}{2}}}_{\text{DEF}} \\ & \cdot\underbrace{\left(\left|\frac{\partial u}{\partial z}\right|^2+\left|\frac{\partial v}{\partial z}\right|^2\right)^{\frac{1}{2}}}_{\text{VWS}} \\ & +\underbrace{C\left[\left(\frac{\partial u}{\partial x}+\frac{\partial v}{\partial y}\right)_{h2}-\left(\frac{\partial u}{\partial x}+\frac{\partial v}{\partial y}\right)_{h1}\right]}_{\text{DVT}} \end{aligned} \quad (1)$$

The subscripts $h1$ and $h2$ represent the selected time interval for the divergence trend. C is a weighting constant to prevent the divergence trend term from dominating the whole Ellord-Knox index.

MoCATI is developed on top of the Ellrod-Knox index. It is a modification of the Ellrod-Knox index including static stability to moderate the mixing of tracer under stable condi-

Table 1. Summary of the performed radiation calls and the applied values [mol/mol] for the active tracers

Call no.	CO_2	O_3	CH_4	N_2O	CFC-11	CFC-12
RAD01	397.34×10^{-6}	Paul et al. (1998)	1.82254×10^{-6}	327.09×10^{-9}	230×10^{-12}	520×10^{-12}
RAD02	interactive	interactive	interactive	interactive	interactive	interactive
RAD03 (O_3)	397.34×10^{-6}	interactive	1.82254×10^{-6}	327.09×10^{-9}	230×10^{-12}	520×10^{-12}
RAD04 (CO_2)	interactive	Paul et al. (1998)	1.82254×10^{-6}	327.09×10^{-9}	230×10^{-12}	520×10^{-12}
RAD05 (CH_4)	397.34×10^{-6}	Paul et al. (1998)	interactive	327.09×10^{-9}	230×10^{-12}	520×10^{-12}
RAD06 (N_2O)	397.34×10^{-6}	Paul et al. (1998)	1.82254×10^{-6}	interactive	230×10^{-12}	520×10^{-12}

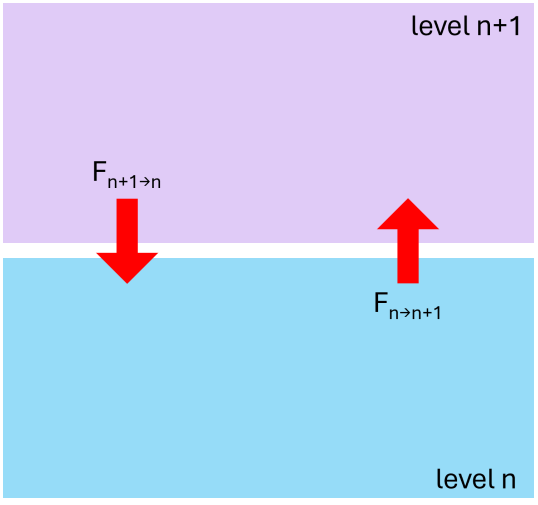

Figure 1. Schematic of the tracer mixing algorithm of the CAT submodel. F represents the flux of mixing and n represents the model vertical level.

tions:

$$\text{MoCATI} = \frac{N_{\text{lim}}^2 - N^2}{N_{\text{lim}}^2} \cdot \text{Ellrod-Knox index} \quad (2)$$

The N^2 is the moist Brunt-Väisälä frequency calculated by the equivalent potential temperature and N_{lim}^2 is a limitation threshold to modify the whole stability term, considering that a stable environment will suppress the formation of turbulence. In addition, the mixing will be switched off above the N_{lim}^2. In order to demonstrate that the stability modification of MoCATI preserves the utility of the original Ellrod-Knox index, statistical tests and frequency distribution analysis are performed. MoCATI shows a comparable performance with the Ellrod-Knox index; details can be found in the Supplement Sect. S1.

A schematic of the tracer mixing algorithm is shown in Fig. 1. The flux of the mixing between level n and level $n+1$ depends on the mixing ratio (χ) and the CAT index at the boundary of both layers. The flux from level n to $n+1$ can be express as:

$$F_{n \to n+1} = \chi \cdot \text{CAT Index}_{\text{boundary}} \quad (3)$$

Table 2. Used values of the namelist parameters.

Parameters	Selected values	Source
C	0.025	Fig. S3
nhours	6	Ellrod and Knox (2010)
N_{lim}^2	6×10^{-4}	Chau et al. (2025)
t_{norm}	15.5	Fig. 2b

The CAT index at the boundary can be calculated by:

$$\text{CAT Index}_{\text{boundary}} = \frac{\text{CAT Index}_n + \text{CAT Index}_{n+1}}{2} \cdot \frac{\Delta t}{t_{\text{norm}}} \quad (4)$$

The Δt is the time step length and the t_{norm} is a time normalization factor. The whole term is used to moderate the strength of mixing.

The CAT submodel allows changes in different parameters via a simple namelist. An example namelist can be found in the electronic supplement. The values used in this study are summarized in Table 2. The constant C in the DVT of the Ellrod-Knox index is selected according to our sensitivity analysis on the frequency distribution (Fig. S3). We found that the suggested values of 0.1 from (Ellrod and Knox, 2010) and 0.01 from Lee et al. (2020) lead to either too strong or too weak DVT compared to the VWS and DEF. The time interval of DVT (nhours) is selected based on (Ellrod and Knox, 2010) and the limitation threshold (N_{lim}^2) is selected based on (Chau et al., 2025). The t_{norm} which moderates the strength of tracer mixing is an empirical value that shown to improve the ozone representation in EMAC (Fig. 2b) against observations (SWOOSH).

2.3.1 Limitations of the CAT approach

Despite the improvements shown in Sect. 3.1, several limitations regarding the current CAT mixing scheme should be noted. The current approach of the CAT mixing scheme assumes the tracer mixing flux is linearly proportional to the magnitude of the CAT index, while the mapping functions between the turbulence strength and turbulence diagnostics are only piecewise linear (Sharman et al., 2006). It should also be noted that this parametrization is specifically tuned for the EMAC model under T42L90MA resolution, which

is one of the most widely used resolutions, especially for long-term climatic studies including the stratosphere. For example, the namelist parameter C in the DVT is resolution-dependent and t_{norm} is an empirical value as well. Application of the CAT submodel to other model setups of EMAC or other climate models will require retuning. Also, water vapour is not treated as a chemical tracer in EMAC but as a thermodynamic quantity (specific humidity) and is therefore excluded in the current version of CAT in order to maintain identical model dynamics for comparison between the simulations under QCTM mode.

3 Results and Discussion

3.1 Comparison of simulated O_3 with SWOOSH observations

In order to examine the performance of the new CAT submodel, a comparison between both simulations and the satellite-based database SWOOSH (Davis et al., 2016) is conducted. Figure 2a and b show the annual mean difference of ozone between both simulations and the SWOOSH. By applying the CAT submodel, the overestimated ozone over the polar regions in the stratosphere is significantly reduced. The vertical mixing by CAT in QCTM-MIX reduces the ozone significantly between 75 to 175 hPa compared to QCTM-NOMIX, the details are discussed further in Sect. 3.2. A previous study from (Righi et al., 2015) shows that EMAC underestimates the ozone hole in Antarctica, causing a warm bias in the southern hemispheric stratosphere. QCTM-MIX shows a better consistency with SWOOSH in this region for ozone. As will be described later, Fig. 8 shows the annual mean difference in the net radiation between both simulations. The local cooling caused by the changes in ozone in this region might partly resolve the warm bias in this region. An extra simulation (QCTM-MIX-ENI) is conducted to show the necessity of the stability modification of MoCATI by using simply the Ellrod-Knox index as the mixing coefficient (the other model setup is identical). Figure 2c shows the annual mean difference of ozone between QCTM-MIX-ENI and SWOOSH. Without the stability modification, ozone is "overmixed" and leads to underestimation in many regions, especially the Northern Hemisphere and the tropics. In order to evaluate whether CAT could improve the representation of ozone climatologically in EMAC, we calculated the normalized root mean square error (RMSE) of all 3 simulations (Table 3). QCTM-MIX shows the lowest normalized RMSE in most of the region except for the Southern Hemisphere. QCTM-MIX-ENI shows the lowest RMSE in the Southern Hemisphere, but shows a larger RMSE in other regions compared to QCTM-NOMIX. These results indicate that QCTM-MIX shows an improvement in all regions compared to QCTM-NOMIX, while QCTM-MIX-ENI improves the most in the Southern Hemisphere, but worsens the representation in other regions compared to QCTM-NOMIX.

Table 3. Root mean square error between simulation and SWOOSH normalized with SWOOSH for global, Northern Hemisphere (NH), Southern Hemisphere (SH) and the tropics. Bold font represents the lowest RMSE.

50–250 hPa	QCTM-NOMIX	QCTM-MIX	QCTM-MIX-ENI
Global	0.4029	**0.3410**	0.3656
NH	0.2782	**0.2720**	0.3474
SH	0.4973	0.3981	**0.3828**
Tropics	0.4196	**0.3952**	0.4593
75–175 hPa	**QCTM-NOMIX**	**QCTM-MIX**	**QCTM-MIX-ENI**
Global	0.4613	**0.3793**	0.3980
NH	0.2894	**0.2703**	0.3687
SH	0.5847	0.4633	**0.4254**
Tropics	0.4616	**0.4439**	0.5190

These results show that with the new mixing parametrization of tracers based on the static stability correction on the Ellrod-Knox index (MoCATI), the representation of ozone in the EMAC model is improved compared to SWOOSH in a climatological sense.

3.2 Difference in tracer distributions

Figure 3 shows the annual zonal mean mixing ratio and difference of O_3, CH_4, CO_2 and N_2O between QCTM-MIX and QCTM-NOMIX to assess the potential impact of tracers by the mixing algorithm of CAT. These major radiatively active gases were selected for the analysis to illustrate the different responses to CAT between spatially variable gases and well-mixed gases. As a result of enabling CAT, the O_3 in the UTLS is significantly reduced, especially in the vicinity of the tropopause with a 10 % to 20 % decrease (except below the tropical tropopause). The changes between 100 to 50 hPa at the extratropics could also be attributed to changes of the tracer gradient by the enhanced vertical mixing at the tropics which leads to enhanced horizontal advection through the shallow branch of the Brewer-Dobson circulation. CAT also changed the O_3 by changing the chemistry (Fig. 4a, b) in the upper stratosphere (above 50 hPa), causing up to 3 % increase, and transport downward across the tropopause to the troposphere with maximum of 9 % increase in the tropical upper troposphere and Southern Hemisphere. In terms of the mixing ratio, the largest absolute difference is located at around 75 hPa in the extratropical region, with up to 320 ppbv reduction of O_3. For CH_4, CAT leads to a significant increase in the UTLS up to 2.5 % or 40 ppbv and a slight loss in the troposphere. The two gases exhibit an opposite behaviour with O_3 decreasing and CH_4 increasing in the UTLS since the O_3 mixing ratio is higher in the UTLS than in the troposphere whereas the CH_4 mixing ratio is higher in the troposphere. O_3 also has a more significant change compared to CH4 due to the steeper gradient. The changes in both gases are stronger in the Southern Hemisphere, potentially

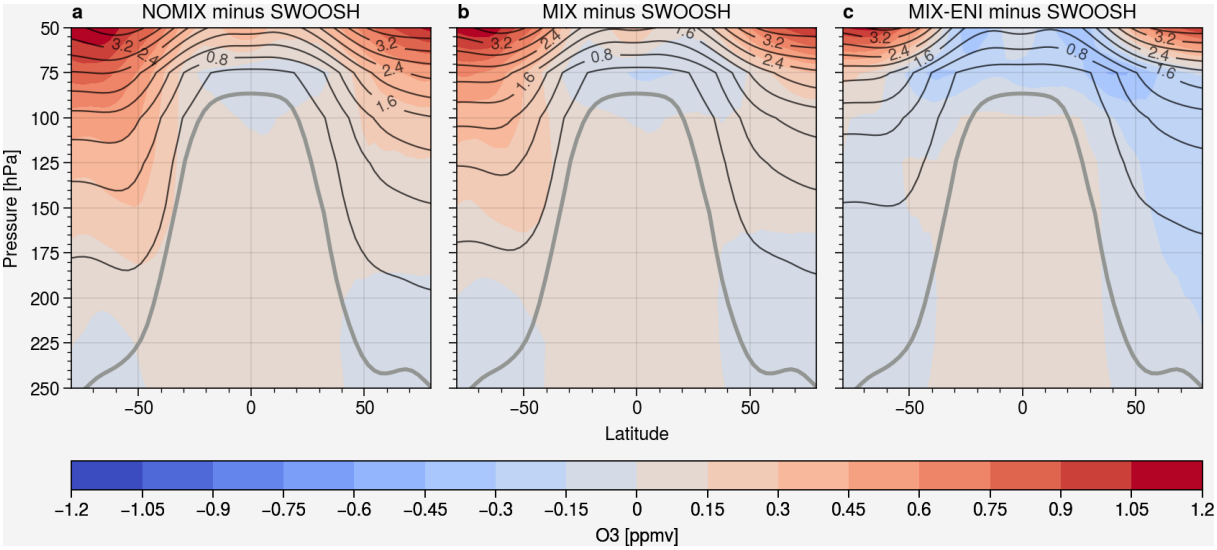

Figure 2. Cross section of the annual ozone zonal mean difference for **(a)** QCTM-NOMIX minus SWOOSH, **(b)** QCTM-MIX minus SWOOSH, and **(c)** QCTM-MIX-ENI minus SWOOSH. The contour lines represent the mixing ratio of O_3 in ppmv of the respective QCTM simulation. The black solid line indicates the PV tropopause in the extratropics and lapse rate tropopause in the tropics.

due to the stronger jet streams and fewer mountains, leading to a stronger vertical wind gradient and resulting in a higher CAT $\text{Index}_{\text{boundary}}$ as in Fig. A1 . For CO_2, since it is well-mixed with a long atmospheric lifetime, the effect of mixing is comparatively weak, given the resulting low vertical gradient. In contrast to this, the effect of CAT mixing on the N_2O mixing ratio is slightly stronger, similar to CH_4, but with a more homogeneous effect on both hemispheres.

To examine whether the differences in the tracer distribution are attributed solely to the mixing of CAT or also influenced by the chemical feedback of other mixed tracers, we analyzed the chemical production and loss terms of ozone as well. The chemistry submodel MECCA (Sander et al., 2011) used in EMAC provided diagnostic output for some of the chemical species. Figure 4 shows the difference (MIX minus NOMIX) in ozone production, total loss and loss by species. With CAT mixing, the production of ozone (Fig. 4a) is reduced and the loss is enhanced (Fig. 4b) at the tropical tropopause, whereas the extra-tropical lower stratosphere (LS) shows an inverse behaviour. These results indicate that the reduction of ozone (Fig. 3) at the tropical tropopause is enhanced by the chemical feedback, whereas the physical mixing is offset by the chemical feedback in the extra-tropical LS.

The chemical loss of ozone (Fig. 4b) is enhanced below the tropical tropopause after including the CAT mixing parametrization. It is mainly contributed by HO_x (Fig. 4e) and $O(^1D)$ (Fig. 4g). Fig. 4g shows the difference in the chemical loss by atomic oxygen. This shows the loss of ozone by removing $O(^1D)$ from the odd oxygen: ozone is photolysed to form $O(^1D)$ via Reaction (R1), $O(^1D)$ is then consumed with H_2O to form OH (Reaction R2). This also partly explains the increase of OH in Fig. S2c in the supplement.

$$O_3 -> [h\nu]O(^1D) + O_2 \quad \text{(R1)}$$

$$O(^1D) + H_2O -> 2OH \quad \text{(R2)}$$

Figure 4e shows the changes in the chemical loss by HO_x. This illustrates the increasing loss of ozone at the tropical tropopause due to the OH / HO_x catalytic cycle. Ozone is destroyed by Equations R3 and R4 with OH / HO_x as a catalyst. This cycle is enhanced due to the increasing HO_x concentration (Fig. S2f in the Supplement).

$$OH + O_3 \rightarrow HO_2 + O_2 \quad \text{(R3)}$$

$$HO_2 + O_3 \rightarrow OH + 2O_2$$

$$\overline{\text{Net}: 2O_3 \rightarrow 3O_2} \quad \text{(R4)}$$

Mixing by CAT also reduces the chemical loss of ozone (Fig. 4b) at the extra-tropical LS ($\sim$ 100 to 50 hPa). Around half of the reduction is due to the reduction of HO_x (Fig. S2f) and NO_x (Fig. S2l and o) in the corresponding region. The reduction of HO_x in the extra-tropics LS and NO_x reduction in the UTLS decelerate the HO_x cycle and NO_x-related cycle. Halogens are responsible for the remaining reduction, especially in the Southern Hemisphere. The vertical mixing evened out the high concentrations at the poles, decelerating the catalytic cycle.

In addition, the change of the chemical regime of ozone is analyzed using the HCHO / NO_2 ratio (Formaldehyde to NO_2 ratio; FNR) and a novel diagnostic $\alpha_{CH_3O_2}$ developed by Nussbaumer et al. (2022). FNR is a commonly used indicator that develops from the principle that formation of tropospheric ozone requires volatile organic compounds (VOCs)

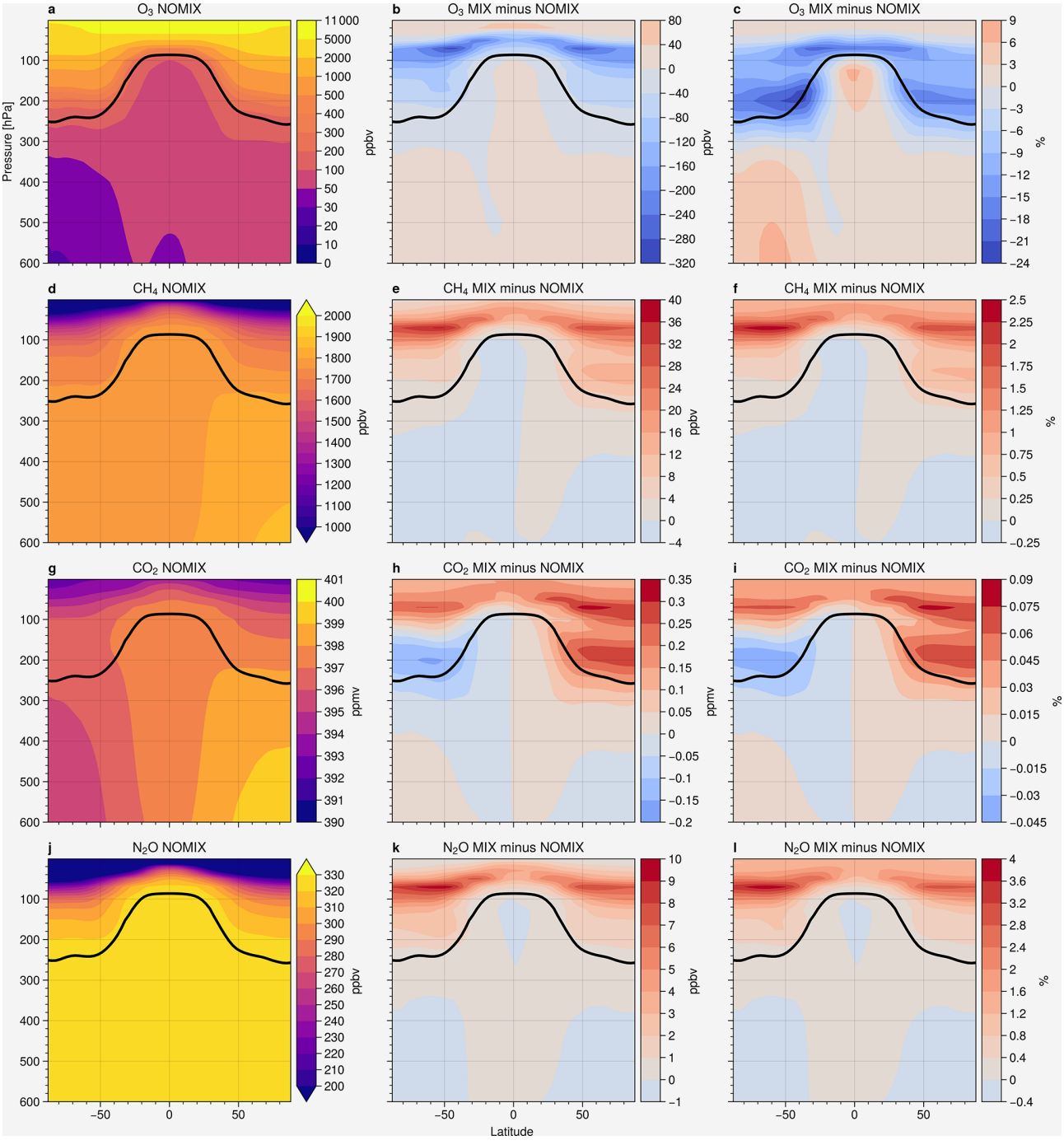

Figure 3. Annual zonal mean O_3, CH_4, CO_2 and N_2O profile of QCTM-NOMIX (first column), absolute difference between both simulations(centre column), and relative percentage difference (right column). The black solid line indicates the PV tropopause in the extratropics and lapse rate tropopause in the tropics.

and NO_x as its precursors (Acdan et al., 2023; Jin et al., 2020; Jiang et al., 2025). HCHO and NO_2 serve as the proxies of the VOCs and NO_x respectively, considering their similar chemical lifetime could better show competition between species (Tonnesen and Dennis, 2000). The lower FNR indicates VOC sensitivity, while the higher FNR indicates NO_x sensitivity. The $\alpha_{CH_3O_2}$ represents the fraction of CH_3O_2 forming HCHO via NO and OH relative to the competing pathway that forms CH_3OOH via HO_2 which could be used to identify the HCHO production pathways. It could also be used to study ozone sensitivity (Nussbaumer et al., 2024). It is based on the concept that the formation of HCHO from

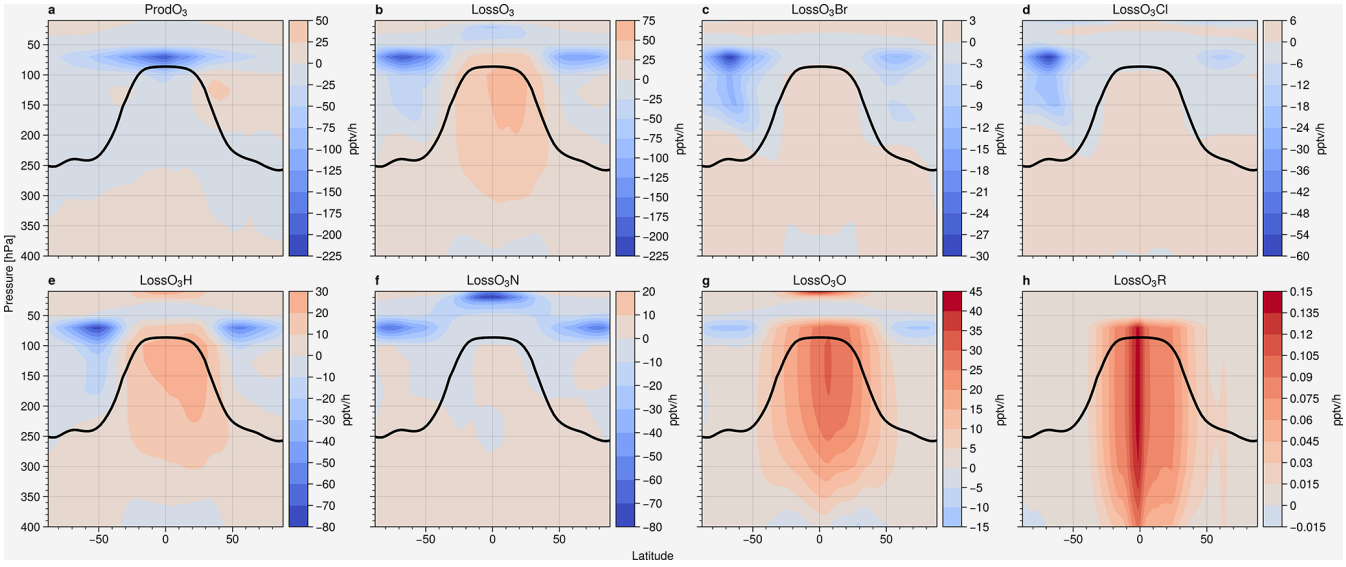

Figure 4. Annual zonal mean difference (MIX – NOMIX) of O_3 chemical production and chemical loss: **(a)** total production, **(b)** total loss, **(c)** loss by bromine, **(d)** loss by chlorine, **(e)** loss by hydrogen species, **(f)** loss by nitrogen species, **(g)** loss by atomic oxygen and **(h)** loss by peroxy radicals. The black solid line indicates the PV tropopause in the extratropics and lapse rate tropopause in the tropics.

CH_3O_2 with NO leads to O_3 production, while the formation of CH_3OOH from CH_3O_2 with HO_2 leads to termination of the HO_x cycle which decelerates the ozone production. The reaction of CH_3O_2 with OH that forms HCHO, which generally only plays a minor role, will not contribute to O_3 formation and therefore will be neglected when studying ozone sensitivity. It can therefore be calculated as shown in Eq. (5):

$$\alpha_{CH_3O_2} = \frac{k_{CH_3O_2+NO} \times [NO]}{k_{CH_3O_2+NO} \times [NO] + k_{CH_3O_2+HO_2} \times [HO_2]} \quad (5)$$

Nussbaumer et al. (2023) shows that both the FNR and $\alpha_{CH_3O_2}$ are good indicators for the ozone chemical regime in the upper troposphere. Fig. 5 shows the 10-year climatology of the $\alpha_{CH_3O_2}$. CAT leads to slight changes in $\alpha_{CH_3O_2}$ in different altitudes. The difference of $\alpha_{CH_3O_2}$ (Fig. 5a) shows a bi-modal distribution at the upper troposphere ($\sim$ 200 hPa) and the lower troposphere ($\sim$ 800 hPa). The Southern Hemisphere exhibits a larger decrease with a maximum of 3 %. The difference even reaches up to 6 % during the JJA season in the southern polar region (not shown). The decreasing $\alpha_{CH_3O_2}$ indicates the decrease of NO and increase of HO_2, which is consistent with Fig. S2l and f and the O_3 is relatively more sensitive to NO_x (less sensitive to VOCs) than without the CAT mixing. Fig. 6 shows the 10-year climatology for the FNR. The Southern Hemisphere depicts a more substantial absolute increase in FNR in the lower troposphere($\sim$ 800 hPa), while the upper troposphere ($\sim$ 200 hPa) shows a percentage increase up to 26 %. The changes above 200 hPa are neglected since the stratospheric ozone chemistry is significantly different than the troposphere. It shows consistent results with the $\alpha_{CH_3O_2}$, the increasing FNR indicates the O_3 chemical regime is becoming relatively more NO_x sensitive (less VOCs sensitive). Both the FNR and $\alpha_{CH_3O_2}$ show that the CAT mixing in the UTLS also affects the tropospheric chemistry.

Furthermore, the chemical lifetime of CH_4 has been analyzed as well. Fig. 7 shows the climatology of the methane lifetime. CAT mixing leads to a significant reduction of the CH_4 lifetime in the UTLS region, the tropics experienced a 15-year ($\sim$ 8 %) decrease. The global atmospheric lifetime of CH_4 also shortened from 7.31 years to 7.24 years. It is mainly due to the change in OH distribution by CAT. Fig. S2c shows that the OH increases mainly in the lower stratosphere with 10 % of increase at the tropical tropopause which coincides with the lifetime profile in Fig. 7. Considering the extremely short atmospheric lifetime of OH, the changes are unlikely to be a direct result of the CAT mixing on OH. It must be a result of either the changes in the OH precursors or sinks. One of the possible pathways is that the increasing OH by $O(^1D)$ leads to a more efficient CH_4 oxidation, which produces more HCHO and HO_2 (based on the lower $\alpha_{CH_3O_2}$). Photolysis of HCHO and HO_2 recycling then generates OH, establishing a HO_x–CH_4–HCHO feedback cycle.

To conclude, the CAT mixing clearly modifies the chemical regime of the O_3 budget, shifting the O_3 to become relatively sensitive to NO_x, as well as reducing the atmospheric lifetime of CH_4 by increasing OH.

3.3 Impact on radiation

The simulation results show that the CAT mixing of tracers leads to a radiative cooling on the global mean radiation fluxes at the top-of-the-atmosphere (TOA) of about 208.9 mW m^{-2} without taking water vapour into account. It

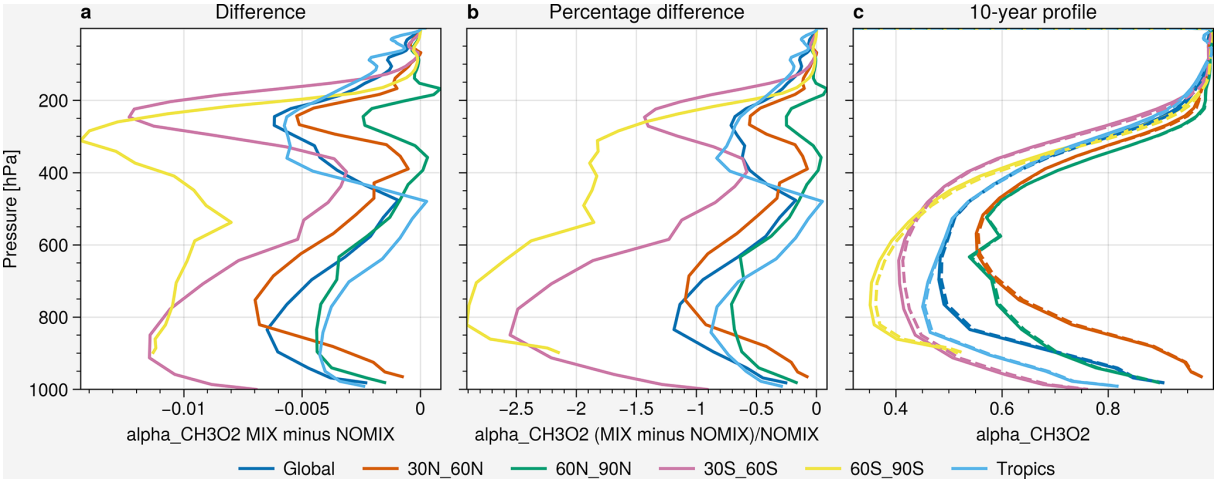

Figure 5. Vertical profile of the 10-year climatology of $\alpha_{CH_3O_2}$ in different regions: **(a)** absolute difference (MIX – NOMIX), **(b)** percentage difference, **(c)** profiles. The solid lines indicates profiles of MIX, the dashed lines indicate profiles of NOMIX. The different colors denote respective latitude bands.

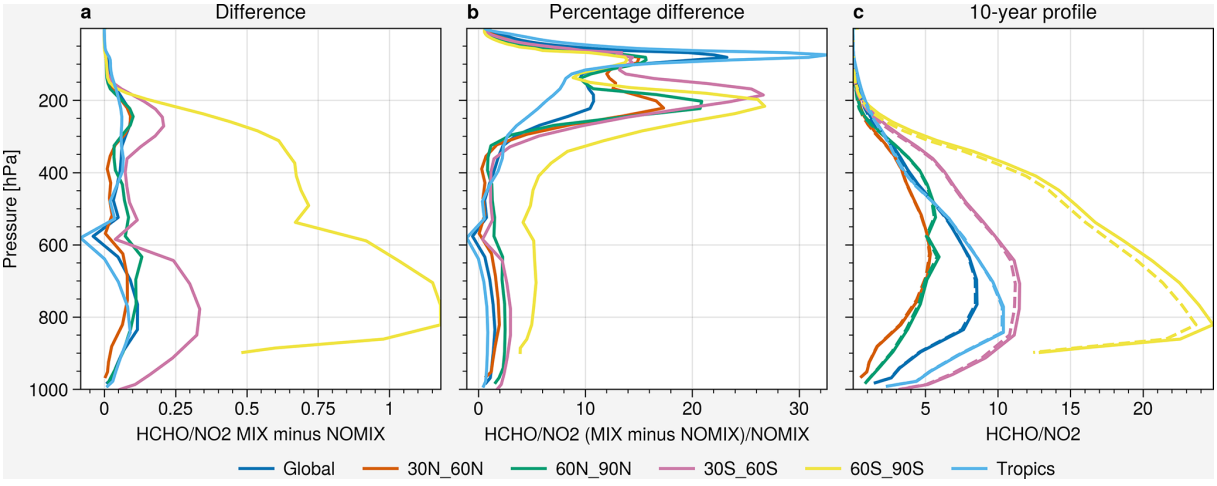

Figure 6. Vertical profile of the 10-year climatology of the HCHO / NO_2 ratio (FNR) in different regions: **(a)** absolute difference (MIX – NOMIX), **(b)** percentage difference, **(c)** profiles. The solid lines indicate profiles of MIX, the dashed lines indicate profiles of NOMIX. The different colors denote respective latitude bands.

is mainly induced by the change in ozone ($-210.5\,\mathrm{mW\,m^{-2}}$). The other major greenhouse gases like CO_2, CH_4 and N_2O have a comparably small impact which either leads to a radiative cooling or heating effect at the TOA. The changes of the annual mean net radiation fluxes of different radiation calls are shown in Figs. 8 and Fig. 9. Each radiation call represents a different greenhouse gas scenario; a summary of the radiation calls is given in Table 1. Figure 8 illustrates the annual zonal mean difference of the net radiation fluxes. In general, CAT mixing leads to cooling above the tropopause and heating in the troposphere (Fig. 8a). It is mainly contributed by ozone (Fig. 8b), with almost identical behaviour as in Fig. 8a. The loss of ozone in the UTLS shown in Fig. 3b, leads to local and TOA radiative cooling as well as heating in the troposphere. CO_2 and CH_4 show mainly an opposite response compared to ozone, while CO_2 has a stronger radiative heating in the Northern Hemisphere, potentially because of anthropogenic activities. N_2O shows a heating effect in almost all altitudes, except for the tropical lower troposphere. Figure 9 shows the annual mean difference of the net radiation fluxes at the TOA and surface. CAT leads to radiative cooling at the TOA and heating at the surface, mainly contributed by ozone. It is more pronounced along the storm tracks, where strong jet stream and associated wind shear favour turbulent mixing in the UTLS. At the TOA, CO_2 leads to cooling in the Southern Hemisphere and heating in the Northern Hemisphere, while the surface shows an inverse behaviour. CH_4 warms the tropics at the TOA, but

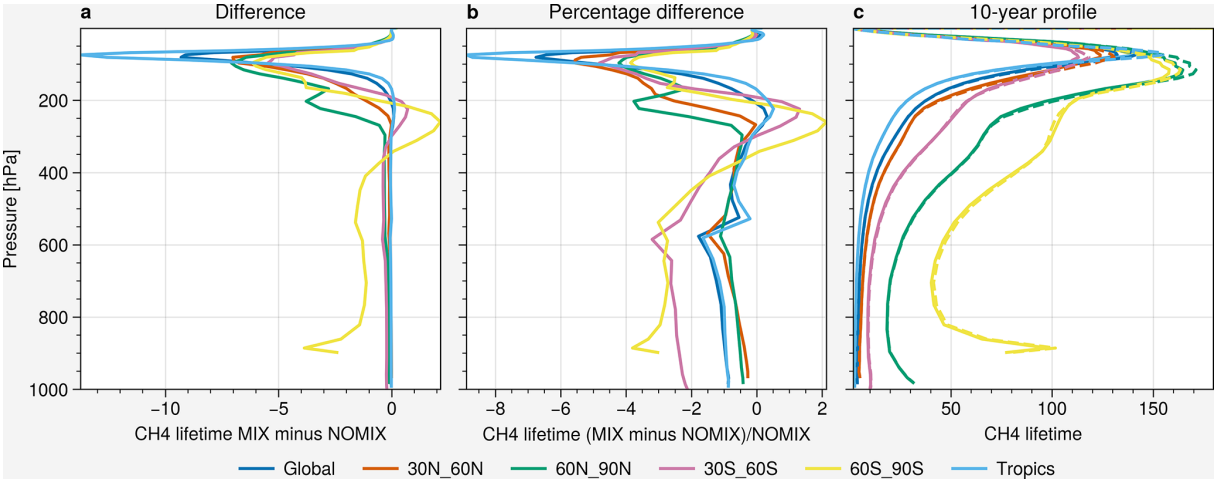

Figure 7. Vertical profile of the 10-year climatology of CH_4 lifetime (year) in different regions: **(a)** absolute difference (MIX – NOMIX), **(b)** percentage difference, **(c)** profiles. The solid lines indicate profiles of MIX, the dashed lines indicate profiles of NOMIX. The different colors denote respective latitude bands.

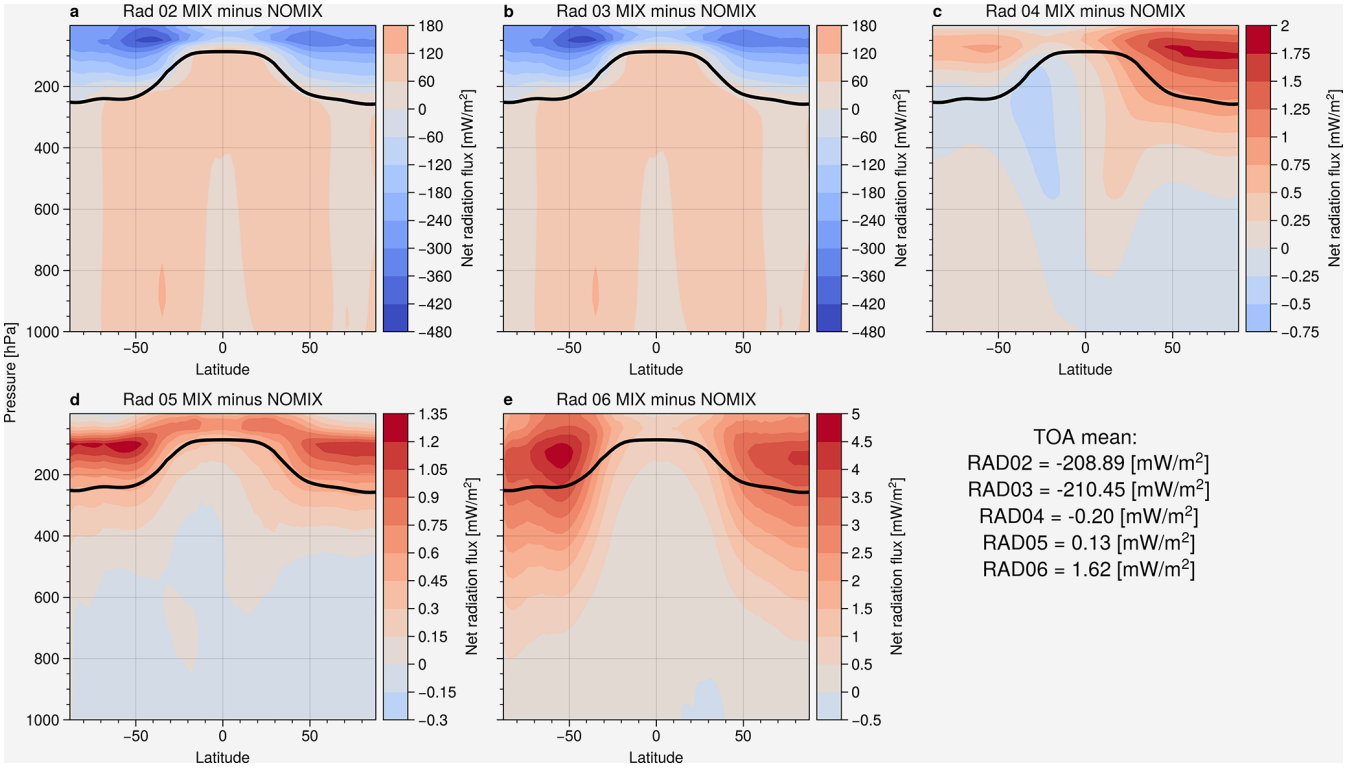

Figure 8. Annual zonal mean difference of net radiation fluxes for different radiation calls between two simulatioins: **(a)** RAD02, **(b)** RAD03 (O_3), **(c)** RAD04 (CO_2), **(d)** RAD05 (CH_4), and **(e)** RAD06 (N_2O). The numerical values given are differences of the global mean TOA radiation. The black solid line indicates the PV tropopause in the extratropics and lapse rate tropopause in the tropics.

cools at the surface. Changes in N_2O result in heating at the TOA and the surface, except for the tropics.

Overall, CAT mixing leads to cooling in the Earth's radiation budget, mainly contributed by O_3, which is a greenhouse gas with spatial variability and also strongly active in the shortwave spectrum. In contrast, well-mixed greenhouse gases like CO_2, CH_4 and N_2O are rather insensitive to CAT mixing, with global mean TOA radiative effects of -0.2, 0.13 and 1.62 mW m^{-2} respectively.

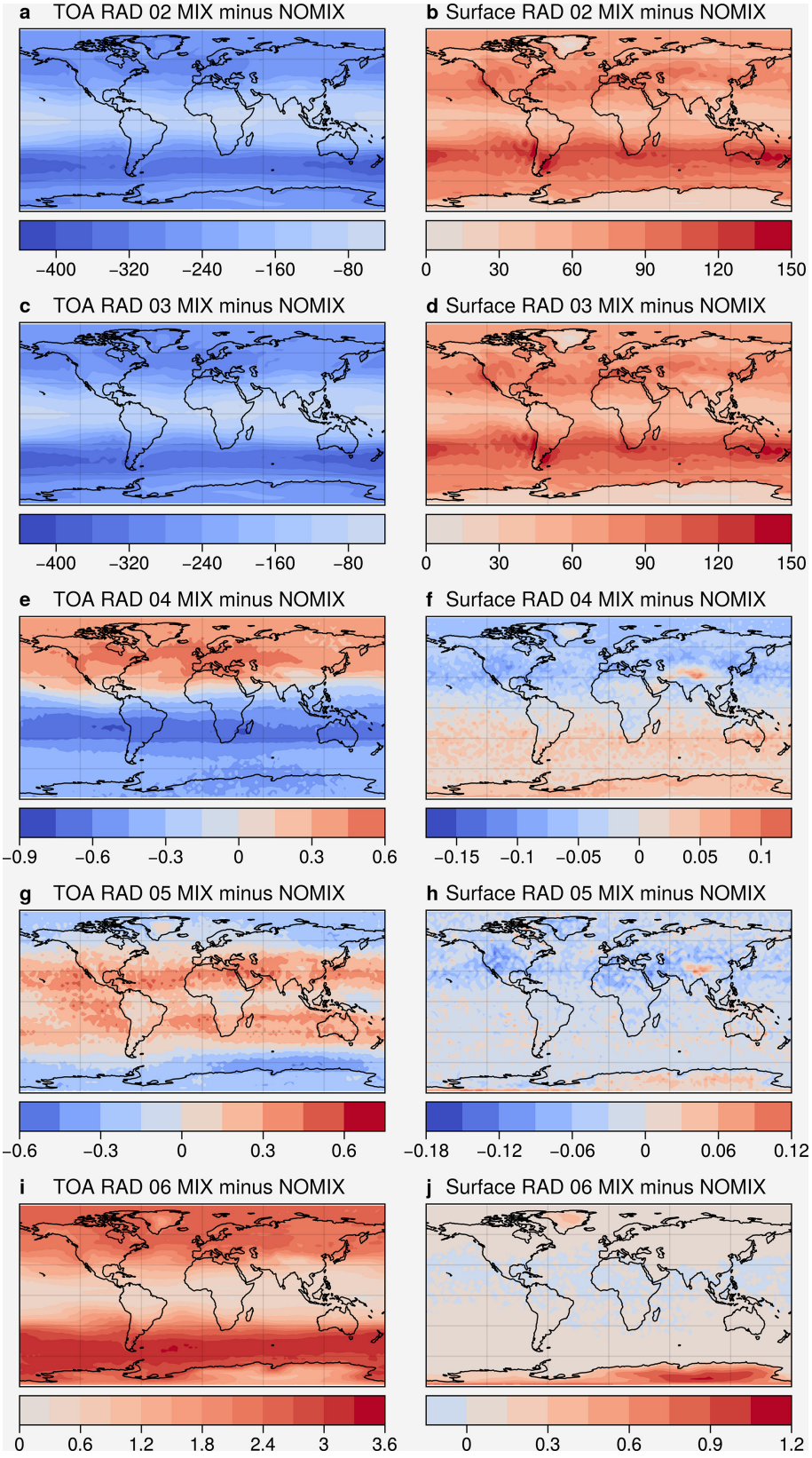

Figure 9. Annual mean difference of net radiation fluxes [mW m^{-2}] at the TOA for **(a)** RAD02, **(c)** RAD03, **(e)** RAD04, **(g)** RAD05, and **(i)** RAD06; and at the surface for **(b)** RAD02, **(d)** RAD03, **(f)** RAD04, **(h)** RAD05, and **(j)** RAD06.

We examined the impact of CAT on tracers and their associated radiative effects. Overall, CAT leads to an increase in outgoing LW radiation at the TOA, corresponding to a cooling effect. It is mainly driven by ozone. The other major greenhouse gases, such as CO_2, CH_4, and N_2O which lead to changes in radiation of TOA are comparatively insensitive to CAT considering they are well-mixed in the atmosphere. A previous study by Riese et al. (2012) shows similar results on the sensitivity of the greenhouse gases by mixing, where water vapour and ozone are notably more sensitive than CH_4 and N_2O. However, due to differences in the mixing parametrization, it resulted in an opposite radiative impact. That study uses the Chemical Lagrangian Model of the Stratosphere (CLaMS) with a mixing algorithm based on atmospheric deformation (McKenna et al., 2002a, b; Konopka et al., 2004). This mixing scheme merges air parcels when they fall below the minimum separation distance. This deformation-induced mixing is a good approximation for stirring and quasi-isentropic mixing in the stably stratified stratosphere. Some more recent studies (Pommrich et al., 2014; Konopka et al., 2019) show that in the previous version of CLaMS which (Riese et al., 2012) were using, the vertical transport within the troposphere is underestimated. This causes the mixing by CLaMS to be mainly attributed to quasi-horizontal isentropic transport which dominates between tropical upper troposphere and extra-tropical lower stratosphere and within the stratosphere, which only reflects part of the potential mixing in the UTLS. The new CAT submodel, on the other hand, parametrizes the mixing by turbulence, a diabatic process that allows exchange across the tropopause. It includes not only the deformation but also vertical wind shear, divergence, and static stability. Also, the CLaMS chemistry is relatively simple compared to EMAC, as well as in describing small-scale dynamics. The mixing scheme of CAT is in turn, more sensitive to vertical mixing, while CLaMS is more sensitive to the isentropic (quasi-horizontal) mixing.

4 Conclusion and Outlook

This study presents a new submodel for parametrizing vertical tracer mixing in the UTLS by Clear Air Turbulence (CAT), developed for the chemistry climate model EMAC, considering the dampening characteristics of the ECHAM5 turbulence scheme above the planetary boundary layer. The CAT mixing scheme is based on a two-layer mixing algorithm and the newly developed turbulence diagnostic MoCATI, which is a modification of the well-known Ellrod-Knox index by introducing static stability into the calculation. We conducted statistical tests and the relative frequency distribution of MoCATI and Ellrod-Knox index. The new index shows a comparable performance as the Ellrod-Knox index.

We performed two simulations (MIX and NOMIX) using the EMAC model in a QCTM configuration to examine the impact of CAT mixing parametrization on tracer distribution and its corresponding radiative impact. CAT leads to significant impacts on the non well-mixed gases like ozone in the UTLS. The changes are contributed by both the physical mixing and the chemical feedback from other tracers. O_3 is significantly reduced in the UTLS and increases in the free troposphere as well as in the mid-stratosphere. The reduction in the tropics is a result of both the physical mixing and chemical feedback from other mixed tracers like odd oxygen and HO_x while the extratropical physical mixing is offset by the chemical feedback not only from odd oxygen and HO_x, but also from halogen species. Other major greenhouse gases including CO_2, CH_4 and N_2O are relatively insensitive to CAT considering their well-mixed characteristics and weak gradients particularly in the UTLS. It also shows that the CAT in the UTLS can change the chemical regime of O_3 not only in the UTLS region, but also in the lower troposphere, by shifting to a relatively more NO_x sensitive (less VOCs sensitive) environment. Methane lifetimes are also found to be shortened from 7.31 years to 7.24 years (especially at the stratosphere with a 15-year difference) because of the more effective HO_x catalytic cycle. CAT mixing also reduces the ozone bias at the polar mid-stratosphere by comparing the results with SWOOSH.

Simulations show that CAT could lead to surface radiative heating and radiative cooling at the TOA. The TOA is expected to be $0.2 W/m^2$ cooler without considering water vapour. It is mostly contributed by ozone since water vapour is not taken into account in the QCTM mode. Other major greenhouse gases show negligible impacts on the radiation budget. Considering the strengthening trend of CAT under climate change, the cooling effect of CAT mixing on tracers could potentially partially offset the warmer climate.

Even though water vapour is not taken into account in the current version of CAT to obtain consistent dynamics in the QCTM mode, it is planned to also consider the potential radiative impact of water vapour by extending the CAT submodel and including the mixing of water vapour and temperature. The water vapour is expected to increase in the UTLS considering its gradient. The moist tropospheric air will be expected to be mixed upward with the dry stratospheric air and may significantly change the radiative budget of the atmosphere. The CAT submodel also has the option to include or combine more turbulence diagnostics (e.g. Graphical Turbulence Guidance from Sharman et al., 2006) in the future, considering the pros and cons of each diagnostic on representing turbulence formed by different mechanisms. However, potential recalibration would be required.

Appendix A

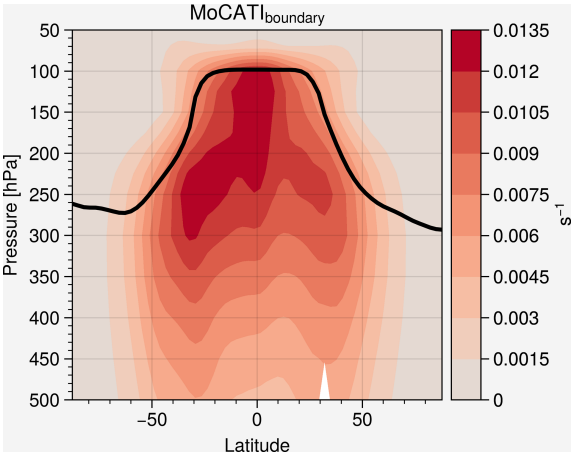

Figure A1. Annual zonal mean of the CAT Index$_{boundary}$ (MoCATI). The black solid line indicates the PV tropopause in the extratropics and lapse rate tropopause in the tropics.

Code availability. The model code of the EMAC chemistry climate model can be obtained by becoming a member of the MESSy consortium as described on the corresponding webpage https://messy-interface.org/, last access: 29 October 2025.

Data availability. Data from this work are available upon request.

Supplement. The supplement related to this article is available online at https://doi.org/10.5194/acp-26-3637-2026-supplement.

Author contributions. CHC and HT conceptualized the study. HT and KK developed the CAT submodel with modifications from CHC. CHC and KK contributed to the submodel evaluation. CHC performed the simulations and analyzed the model results. CHC drafted the manuscript. CHC, HT, and PH discussed the results. All co-authors contributed to the review and final editing of the manuscript.

Competing interests. The contact author has declared that none of the authors has any competing interests.

Disclaimer. Publisher's note: Copernicus Publications remains neutral with regard to jurisdictional claims made in the text, published maps, institutional affiliations, or any other geographical representation in this paper. The authors bear the ultimate responsibility for providing appropriate place names. Views expressed in the text are those of the authors and do not necessarily reflect the views of the publisher.

Special issue statement. This article is part of the special issue "The tropopause region in a changing atmosphere (TPChange) (ACP/AMT/GMD/WCD inter-journal SI)". It is not associated with a conference.

Acknowledgements. This work has been funded by the Deutsche Forschungsgemeinschaft (DFG, German Research Foundation) – TRR 301 – Project-ID 428312742 (project B01). The simulations were conducted using the supercomputer MOGON-NHR of Johannes Gutenberg University Mainz (https://hpc.uni-mainz.de/, last access: 15 September 2025).

Financial support. This research has been supported by the Deutsche Forschungsgemeinschaft (grant no. Project-ID 428312742).

This open-access publication was funded by Johannes Gutenberg University Mainz.

Review statement. This paper was edited by Huilin Chen and reviewed by two anonymous referees.

References

Acdan, J. J. M., Pierce, R. B., Dickens, A. F., Adelman, Z., and Nergui, T.: Examining TROPOMI formaldehyde to nitrogen dioxide ratios in the Lake Michigan region: implications for ozone exceedances, Atmos. Chem. Phys., 23, 7867–7885, https://doi.org/10.5194/acp-23-7867-2023, 2023.

Chau, C. H., Hoor, P., and Tost, H.: Simulated mixing in the UTLS by small-scale turbulence using multi-scale chemistry-climate model MECO(n), Atmos. Chem. Phys., 25, 13123–13140, https://doi.org/10.5194/acp-25-13123-2025, 2025.

Davis, S. M., Rosenlof, K. H., Hassler, B., Hurst, D. F., Read, W. G., Vömel, H., Selkirk, H., Fujiwara, M., and Damadeo, R.: The Stratospheric Water and Ozone Satellite Homogenized (SWOOSH) database: a long-term database for climate studies, Earth Syst. Sci. Data, 8, 461–490, https://doi.org/10.5194/essd-8-461-2016, 2016.

Deckert, R., Jöckel, P., Grewe, V., Gottschaldt, K.-D., and Hoor, P.: A quasi chemistry-transport model mode for EMAC, Geosci. Model Dev., 4, 195–206, https://doi.org/10.5194/gmd-4-195-2011, 2011.

Dee, D. P., Uppala, S. M., Simmons, A. J., Berrisford, P., Poli, P., Kobayashi, S., Andrae, U., Balmaseda, M. A., Balsamo, G., Bauer, P., Bechtold, P., Beljaars, A. C. M., van de Berg, L., Bidlot, J., Bormann, N., Delsol, C., Dragani, R., Fuentes, M., Geer, A. J., Haimberger, L., Healy, S. B., Hersbach, H., Hólm, E. V., Isaksen, L., Kållberg, P., Köhler, M., Matricardi, M., McNally, A. P., Monge-Sanz, B. M., Morcrette, J.-J., Park, B.-K., Peubey, C., de Rosnay, P., Tavolato, C., Thépaut, J.-N., and Vitart, F.: The ERA-Interim reanalysis: configuration and performance of the data assimilation system, Q. J. Roy. Meteorol. Soc., 137, 553–597, https://doi.org/10.1002/qj.828, 2011.

Dietmüller, S., Jöckel, P., Tost, H., Kunze, M., Gellhorn, C., Brinkop, S., Frömming, C., Ponater, M., Steil, B., Lauer, A., and Hendricks, J.: A new radiation infrastructure for the Modular Earth Submodel System (MESSy, based on version 2.51), Geosci. Model Dev., 9, 2209–2222, https://doi.org/10.5194/gmd-9-2209-2016, 2016.

Dutton, J. A. and Panofsky, H. A.: Clear Air Turbulence: A Mystery May Be Unfolding, Science, 167, 937–944, https://doi.org/10.1126/science.167.3920.937, 1970.

Ellrod, G., Lester, P., and Ehernberger, L.: CLEAR AIR TURBULENCE, in: Encyclopedia of Atmospheric Sciences, edited by Holton, J. R., 393–403, Academic Press, Oxford, ISBN 978-0-12-227090-1, https://doi.org/10.1016/B0-12-227090-8/00104-4, 2003.

Ellrod, G. P. and Knapp, D. I.: An Objective Clear-Air Turbulence Forecasting Technique: Verification and Operational Use, Weather Forecast., 7, 150–165, https://doi.org/10.1175/1520-0434(1992)007<0150:AOCATF>2.0.CO;2, 1992.

Ellrod, G. P. and Knox, J. A.: Improvements to an Operational Clear-Air Turbulence Diagnostic Index by Addition of a Divergence Trend Term, Weather Forecast., 25, 789–798, https://doi.org/10.1175/2009WAF2222290.1, 2010.

Esler, J. G. and Polvani, L. M.: Kelvin–Helmholtz Instability of Potential Vorticity Layers: A Route to Mixing, J. Atmos. Sci., 61, 1392–1405, https://doi.org/10.1175/1520-0469(2004)061<1392:KIOPVL>2.0.CO;2, 2004.

Eyring, V., Lamarque, J.-F., Hess, P., Arfeuille, F., Bowman, K., Chipperfiel, M. P., Duncan, B., Fiore, A., Gettelman, A., Giorgetta, M., Granier, C., Hegglin, M., Kinnison, D., Kunze, M., Langematz, U., Luo, B., Martin, R., Matthes, K., Newman, P., and Young, P. J.: Overview of IGAC/SPARC Chemistry-Climate Model Initiative (CCMI) community simulations in support of upcoming ozone and climate assessments, SPARC Newsletter, 40, 48–66, 2013.

Forster, P., Storelvmo, T., Armour, K., Collins, W., Dufresne, J.-L., Frame, D., Lunt, D., Mauritsen, T., Palmer, M., Watanabe, M., Wild, M., and Zhang, H.: Chap. 7, The Earth's energy budget, climate feedbacks, and climate sensitivity, Climate Change 2021: The Physical Science Basis. Contribution of Working Group I to the Sixth Assessment Report of the Intergovernmental Panel on Climate Change, https://doi.org/10.25455/wgtn.16869671.v1, 2021.

Forster, P. M. and Shine, K. P.: Radiative forcing and temperature trends from stratospheric ozone changes, J. Geophys. Res.-Atmos., 102, 10841–10855, https://doi.org/10.1029/96JD03510, 1997.

Forster, P. M. and Shine, K. P.: Stratospheric water vapour changes as a possible contributor to observed stratospheric cooling, Geophys. Res. Lett., 26, 3309–3312, https://doi.org/10.1029/1999GL010487, 1999.

Giorgetta, M. A., Manzini, E., Roeckner, E., Esch, M., and Bengtsson, L.: Climatology and Forcing of the Quasi-Biennial Oscillation in the MAECHAM5 Model, J. Clim., 19, 3882–3901, https://doi.org/10.1175/JCLI3830.1, 2006.

Holton, J. R., Haynes, P. H., McIntyre, M. E., Douglass, A. R., Rood, R. B., and Pfister, L.: Stratosphere-troposphere exchange, Rev. Geophys., 33, 403–439, https://doi.org/10.1029/95RG02097, 1995.

Hu, B., Tang, J., Ding, J., and Liu, G.: Regional downscaled future change of clear-air turbulence over East Asia under RCP8.5 scenario within the CORDEX-EA-II project, Int. J. Climatol., 41, 5022–5035, https://doi.org/10.1002/joc.7114, 2021.

Jiang, Z., Wang, S., Yan, Y., Zhang, S., Xue, R., Gu, C., Zhu, J., Liu, J., and Zhou, B.: Constructing the 3D Spatial Distribution of the HCHO/NO2 Ratio via Satellite Observation and Machine Learning Model, Environ. Sci. Technol., 59, 4047–4058, https://doi.org/10.1021/acs.est.4c12362, pMID: 39977671, 2025.

Jin, X., Fiore, A., Boersma, K. F., Smedt, I. D., and Valin, L.: Inferring Changes in Summertime Surface Ozone–NO_x–VOC Chemistry over U.S. Urban Areas from Two Decades of Satellite and Ground-Based Observations, Environ. Sci. Technol., 54, 6518–6529, https://doi.org/10.1021/acs.est.9b07785, pMID: 32348127, 2020.

Jöckel, P., Sander, R., Kerkweg, A., Tost, H., and Lelieveld, J.: Technical Note: The Modular Earth Submodel System (MESSy) – a new approach towards Earth System Modeling, Atmos. Chem. Phys., 5, 433–444, https://doi.org/10.5194/acp-5-433-2005, 2005.

Jöckel, P., Tost, H., Pozzer, A., Brühl, C., Buchholz, J., Ganzeveld, L., Hoor, P., Kerkweg, A., Lawrence, M. G., Sander, R., Steil, B., Stiller, G., Tanarhte, M., Taraborrelli, D., van Aardenne, J., and Lelieveld, J.: The atmospheric chemistry general circulation model ECHAM5/MESSy1: consistent simulation of ozone from the surface to the mesosphere, Atmos. Chem. Phys., 6, 5067–5104, https://doi.org/10.5194/acp-6-5067-2006, 2006.

Jöckel, P., Kerkweg, A., Pozzer, A., Sander, R., Tost, H., Riede, H., Baumgaertner, A., Gromov, S., and Kern, B.: Development cycle 2 of the Modular Earth Submodel System (MESSy2), Geosci. Model Dev., 3, 717–752, https://doi.org/10.5194/gmd-3-717-2010, 2010.

Jöckel, P., Tost, H., Pozzer, A., Kunze, M., Kirner, O., Brenninkmeijer, C. A. M., Brinkop, S., Cai, D. S., Dyroff, C., Eckstein, J., Frank, F., Garny, H., Gottschaldt, K.-D., Graf, P., Grewe, V., Kerkweg, A., Kern, B., Matthes, S., Mertens, M., Meul, S., Neumaier, M., Nützel, M., Oberländer-Hayn, S., Ruhnke, R., Runde, T., Sander, R., Scharffe, D., and Zahn, A.: Earth System Chemistry integrated Modelling (ESCiMo) with the Modular Earth Submodel System (MESSy) version 2.51, Geosci. Model Dev., 9, 1153–1200, https://doi.org/10.5194/gmd-9-1153-2016, 2016.

Kaluza, T., Kunkel, D., and Hoor, P.: On the occurrence of strong vertical wind shear in the tropopause region: a 10-year ERA5 northern hemispheric study, Weather Clim. Dynam., 2, 631–651, https://doi.org/10.5194/wcd-2-631-2021, 2021.

Konopka, P., Steinhorst, H.-M., Grooß, J.-U., Günther, G., Müller, R., Elkins, J. W., Jost, H.-J., Richard, E., Schmidt, U., Toon, G., and McKenna, D. S.: Mixing and ozone loss in the 1999–2000 Arctic vortex: Simulations with the three-dimensional Chemical Lagrangian Model of the Stratosphere (CLaMS), J. Geophys. Res.-Atmos., 109, https://doi.org/10.1029/2003JD003792, 2004.

Konopka, P., Tao, M., Ploeger, F., Diallo, M., and Riese, M.: Tropospheric mixing and parametrization of unresolved convective updrafts as implemented in the Chemical Lagrangian Model of the Stratosphere (CLaMS v2.0), Geosci.Model Dev., 12, 2441–2462, https://doi.org/10.5194/gmd-12-2441-2019, 2019.

Kunkel, D., Hoor, P., Kaluza, T., Ungermann, J., Kluschat, B., Giez, A., Lachnitt, H.-C., Kaufmann, M., and Riese, M.: Evidence

of small-scale quasi-isentropic mixing in ridges of extratropical baroclinic waves, Atmos. Chem. Phys., 19, 12607–12630, https://doi.org/10.5194/acp-19-12607-2019, 2019.

Lacis, A. A., Wuebbles, D. J., and Logan, J. A.: Radiative forcing of climate by changes in the vertical distribution of ozone, J. Geophys. Res.-Atmos., 95, 9971–9981, https://doi.org/10.1029/JD095iD07p09971, 1990.

Lee, S. H., Williams, P. D., and Frame, T. H.: Increased shear in the North Atlantic upper-level jet stream over the past four decades, Nature, 572, 639–642, 2019.

Lee, D.-B., Chun, H.-Y., and Kim, J.-H.: Evaluation of Multimodel-Based Ensemble Forecasts for Clear-Air Turbulence, Weather Forecast., 35, 507–521, https://doi.org/10.1175/WAF-D-19-0155.1, 2020.

McKenna, D. S., Grooß, J.-U., Günther, G., Konopka, P., Müller, R., Carver, G., and Sasano, Y.: A new Chemical Lagrangian Model of the Stratosphere (CLaMS) 2. Formulation of chemistry scheme and initialization, J. Geophys. Res.-Atmos., 107, 4256, https://doi.org/10.1029/2000JD000113, 2002a.

McKenna, D. S., Konopka, P., Grooß, J.-U., Günther, G., Müller, R., Spang, R., Offermann, D., and Orsolini, Y.: A new Chemical Lagrangian Model of the Stratosphere (CLaMS) 1. Formulation of advection and mixing, J. Geophys. Res.-Atmos., 107, 309, https://doi.org/10.1029/2000JD000114, 2002b.

Nussbaumer, C. M., Pozzer, A., Tadic, I., Röder, L., Obersteiner, F., Harder, H., Lelieveld, J., and Fischer, H.: Tropospheric ozone production and chemical regime analysis during the COVID-19 lockdown over Europe, Atmos. Chem. Phys., 22, 6151–6165, https://doi.org/10.5194/acp-22-6151-2022, 2022.

Nussbaumer, C. M., Fischer, H., Lelieveld, J., and Pozzer, A.: What controls ozone sensitivity in the upper tropical troposphere?, Atmos. Chem. Phys., 23, 12651–12669, https://doi.org/10.5194/acp-23-12651-2023, 2023.

Nussbaumer, C. M., Kohl, M., Pozzer, A., Tadic, I., Rohloff, R., Marno, D., Harder, H., Ziereis, H., Zahn, A., Obersteiner, F., Hofzumahaus, A., Fuchs, H., Künstler, C., Brune, W. H., Ryerson, T. B., Peischl, J., Thompson, C. R., Bourgeois, I., Lelieveld, J., and Fischer, H.: Ozone Formation Sensitivity to Precursors and Lightning in the Tropical Troposphere Based on Airborne Observations, J. Geophys. Res.-Atmos., 129, e2024JD041168, https://doi.org/10.1029/2024JD041168, 2024.

Paul, J., Fortuin, F., and Kelder, H.: An ozone climatology based on ozonesonde and satellite measurements, J. Geophys. Res.-Atmos., 103, 31709–31734, https://doi.org/10.1029/1998JD200008, 1998.

Plummer, D., Nagashima, T., Tilmes, S., Archibald, A., Chiodo, G., Fadnavis, S., Garny, H., Josse, B., Kim, J., Lamarque, J.-F., Morgenstern, O., Murray, L., Orbe, C., Tai, A., Chipperfield, M., Funke, B., Juckes, M., Kinnison, D., Kunze, M., Luo, B., Matthes, K., Newman, P. A., Pascoe, C., and Peter, T.: CCMI-2022: A new set of Chemistry-Climate Model Initiative (CCMI) community simulations to update the assessment of models and support upcoming Ozone Assessment activities, SPARC Newsletter, 57, 22–30, 2021.

Pommrich, R., Müller, R., Grooß, J.-U., Konopka, P., Ploeger, F., Vogel, B., Tao, M., Hoppe, C. M., Günther, G., Spelten, N., Hoffmann, L., Pumphrey, H.-C., Viciani, S., D'Amato, F., Volk, C. M., Hoor, P., Schlager, H., and Riese, M.: Tropical troposphere to stratosphere transport of carbon monoxide and long-lived trace species in the Chemical Lagrangian Model of the Stratosphere (CLaMS), Geosci. Model Dev., 7, 2895–2916, https://doi.org/10.5194/gmd-7-2895-2014, 2014.

Randel, W. J., Wu, F., and Forster, P.: The Extratropical Tropopause Inversion Layer: Global Observations with GPS Data, and a Radiative Forcing Mechanism, J. Atmos. Sci., 64, 4489–4496, https://doi.org/10.1175/2007JAS2412.1, 2007.

Richardson, L. F.: The supply of energy from and to atmospheric eddies, Proc. Roy. Soc. Lond. Ser. A, 97, 354–373, 1920.

Riese, M., Ploeger, F., Rap, A., Vogel, B., Konopka, P., Dameris, M., and Forster, P.: Impact of uncertainties in atmospheric mixing on simulated UTLS composition and related radiative effects, J. Geophys. Res.-Atmos., 117, https://doi.org/10.1029/2012JD017751, 2012.

Righi, M., Eyring, V., Gottschaldt, K.-D., Klinger, C., Frank, F., Jöckel, P., and Cionni, I.: Quantitative evaluation of ozone and selected climate parameters in a set of EMAC simulations, Geosci. Model Dev., 8, 733–768, https://doi.org/10.5194/gmd-8-733-2015, 2015.

Roeckner, E., Bäuml, G., Bonaventura, L., Brokopf, R., Esch, M., Giorgetta, M., Hagemann, S., Kirchner, I., Kornblueh, L., Manzini, E., Schlese, U., and Schulzweida, U.: The atmospheric general circulation model ECHAM 5, PART I: Model description, Max-Planck-Institut für Meteorologie, https://pure.mpg.de/pubman/faces/ViewItemOverviewPage.jsp?itemId=item_995269 (last access: 10 March 2026), 2003.

Sander, R., Baumgaertner, A., Gromov, S., Harder, H., Jöckel, P., Kerkweg, A., Kubistin, D., Regelin, E., Riede, H., Sandu, A., Taraborrelli, D., Tost, H., and Xie, Z.-Q.: The atmospheric chemistry box model CAABA/MECCA-3.0, Geosci. Model Dev., 4, 373–380, https://doi.org/10.5194/gmd-4-373-2011, 2011.

Sharman, R., Tebaldi, C., Wiener, G., and Wolff, J.: An Integrated Approach to Mid- and Upper-Level Turbulence Forecasting, Weather Forecast., 21, 268–287, https://doi.org/10.1175/WAF924.1, 2006.

Smith, I. H., Williams, P. D., and Schiemann, R.: Clear-air turbulence trends over the North Atlantic in high-resolution climate models, Clim. Dynam., 61, 3063–3079, 2023.

Solomon, S., Rosenlof, K. H., Portmann, R. W., Daniel, J. S., Davis, S. M., Sanford, T. J., and Plattner, G.-K.: Contributions of Stratospheric Water Vapor to Decadal Changes in the Rate of Global Warming, Science, 327, 1219–1223, https://doi.org/10.1126/science.1182488, 2010.

Stevenson, D. S., Dentener, F. J., Schultz, M. G., Ellingsen, K., van Noije, T. P. C., Wild, O., Zeng, G., Amann, M., Atherton, C. S., Bell, N., Bergmann, D. J., Bey, I., Butler, T., Cofala, J., Collins, W. J., Derwent, R. G., Doherty, R. M., Drevet, J., Eskes, H. J., Fiore, A. M., Gauss, M., Hauglustaine, D. A., Horowitz, L. W., Isaksen, I. S. A., Krol, M. C., Lamarque, J.-F., Lawrence, M. G., Montanaro, V., Müller, J.-F., Pitari, G., Prather, M. J., Pyle, J. A., Rast, S., Rodriguez, J. M., Sanderson, M. G., Savage, N. H., Shindell, D. T., Strahan, S. E., Sudo, K., and Szopa, S.: Multimodel ensemble simulations of present-day and near-future tropospheric ozone, J. Geophys. Res.-Atmos., 111, https://doi.org/10.1029/2005JD006338, 2006.

Stohl, A., Bonasoni, P., Cristofanelli, P., Collins, W., Feichter, J., Frank, A., Forster, C., Gerasopoulos, E., Gäggeler, H., James, P., Kentarchos, T., Kromp-Kolb, H., Krüger, B., Land, C., Meloen, J., Papayannis, A., Priller, A., Seibert, P., Sprenger, M.,

Roelofs, G. J., Scheel, H. E., Schnabel, C., Siegmund, P., Tobler, L., Trickl, T., Wernli, H., Wirth, V., Zanis, P., and Zerefos, C.: Stratosphere-troposphere exchange: A review, and what we have learned from STACCATO, J. Geophys. Res.-Atmos., 108, https://doi.org/10.1029/2002JD002490, 2003.

Taylor, K., Williamson, D., and Zwiers, F.: AMIP II Sea Surface Temperature and Sea Ice Concentration Boundary Conditions, PCMDI Rep., 60, 2000.

Tonnesen, G. S. and Dennis, R. L.: Analysis of radical propagation efficiency to assess ozone sensitivity to hydrocarbons and NO_x: 2. Long-lived species as indicators of ozone concentration sensitivity, J. Geophys. Res.-Atmos., 105, 9227–9241, https://doi.org/10.1029/1999JD900372, 2000.

Traub, M. and Lelieveld, J.: Cross-tropopause transport over the eastern Mediterranean, J. Geophys. Res., 108, 4712, https://doi.org/10.1029/2003JD003754, 2003.

Watkins, C. and Browning, K.: The detection of clear air turbulence by radar, Phys. Technol., 4, 28–61, https://doi.org/10.1088/0305-4624/4/1/I01, 1973.

Williams, P. D.: Increased light, moderate, and severe clear-air turbulence in response to climate change, Adv. Atmos. Sci., 34, 576–586, 2017.

Williams, P. D. and Joshi, M. M.: Intensification of winter transatlantic aviation turbulence in response to climate change, Nat. Clim. Change, 3, 644–648, 2013.

Williams, P. D. and Storer, L. N.: Can a climate model successfully diagnose clear-air turbulence and its response to climate change?, Q. J. Roy. Meteorol. Soc., 148, 1424–1438, https://doi.org/10.1002/qj.4270, 2022.